NDT net
e-Journal of Nondestructive Testing - ISSN 1435-4934 - www.ndt.net
15th Conference on Industrial Computed Tomography, Wels, Austria (iCT 2026), www.fh-ooe.at/ict-conference-2026

Spectral X-ray micro-CT Imaging of Rechargeable Alkaline Batteries

Andrew Coathup[1,2], Benedetto Bozzini[3], Francesco Brun[1,4], Renato Huber[5], Chuljung Kim[5], Lucia Mancini[6], Emanuele Marini[5], Luca Brombal[1,2]

[1]National Institute for Nuclear Physics (INFN), Division of Trieste, Via A. Valerio 2, 34127 Trieste, Italy
[2]University of Trieste, Department of Physics, Via A. Valerio 2, 34127 Trieste, Italy
[3]Department of Energy, Politecnico di Milano, v. Lambruschini 4, 20156 Milano, Italy
[4]University of Trieste, Department of Engineering and Architecture, via A. Valerio 10, 34127, Trieste, Italy
[5]Center for Solar Energy and Hydrogen Research, Baden-Württemberg (ZSW), Ulm, Germany
[6]Department of Materials, Slovenian National Building and Civil Engineering Institute (ZAG), Dimičeva ulica 12, 1000 Ljubljana, Slovenia

Abstract

Rechargeable alkaline batteries (RABs) represent a promising post-lithium energy storage technology owing to their intrinsic safety, use of sustainable materials, and compatibility with existing battery manufacturing infrastructure. However, their commercial deployment remains limited by insufficient understanding of ageing and degradation mechanisms. In this work, spectral X-ray micro-computed tomography (S-XμCT) is employed to non-destructively investigate pristine and aged Mn–Bi-based RABs, with the aim of resolving ageing-induced changes. A spectral photon-counting detector was used to acquire multi-energy datasets, which were then processed and decomposed into material-specific volumes corresponding to carbon, manganese, and bismuth. Stability and reproducibility testing confirmed the robustness of the S-XμCT acquisition and decomposition process. Quantitative image analysis revealed a pronounced increase in the number of clustered features in aged samples, strongly localized near the anode interface, with the bismuth specific volume providing improved discrimination compared to the traditional attenuation volume. These results highlight the added value of S-XμCT for material-specific, volumetric assessment of degradation phenomena in rechargeable alkaline batteries and suggests its potential as a non-destructive diagnostic tool for battery ageing studies.

Keywords: spectral X-ray micro-CT, material decomposition, rechargeable alkaline batteries, cyclability

1 Introduction

Post-lithium batteries represent a highly promising technology, due to their potential to overcome the sustainability, cost and safety issues of present-day lithium-based systems [1]. Rechargeable Alkaline Batteries (RABs) are particularly promising as they are one of the few actively researched post-Li technologies that feature: (i) power and energy density appropriate for stationary applications; (ii) intrinsic safety, as they do not contain combustible or high-energy electrode materials and use an aqueous electrolyte; and (iii) manufacturing with non-toxic and sustainable raw materials. Moreover, by formulating the electrode materials as slurries that can be tape-cast, state-of-the-art Lithium-Ion Batteries (LIBs) gigafactory fabrication lines can be readily adapted for RAB production. However, despite these advantages, no commercial RAB products currently exist, due in large part to durability issues.

The use of additives in the MnO cathode, in particular Bi-based oxides, has been shown to improve cyclability, although the underlying mechanisms remain poorly understood. In this context, our group investigates the role of Bi in stabilizing the redox of MnO_2, including the anodic and cathodic electrochemistry of the Mn-Bi system in aqueous alkaline electrolytes, as well as the structural and morphochemical evolution of the cathodes. One critical aspect is the architectural evolution of the MnO_2/Bi_2O_3/carbon composite electrodes, including variations in particle-size distribution, porosity and tortuosity [2]. This plays a key functional role and spectral X-ray micro-CT (S-XμCT), with its ability to perform material decomposition, could be an important tool to build the required, and to this point unavailable, knowledge base. The goal of this work is to assess, ex situ, the morphology and texture of Mn-Bi cathodes both in pristine state and after extended cycling under realistic environmental conditions.

2 Methodology

The spectral X-ray micro-computed tomography (S-XμCT) technique was applied to a battery sample in both before (pristine) and after (aged) cycling to obtain a non-destructive, three-dimensional morphochemical characterization. The technique enables simultaneous visualization of individual battery components and the full cell architecture, providing both conventional X-ray attenuation contrast and material-specific information at the microscale through spectral decomposition.

The cathode pellet was prepared by mixing and pressing a powder blend consisting of 38 wt% α-manganese, 47.5 wt% carbon black (C65), 9.5 wt% bismuth, and 5 wt% PTFE binder. After the initial S-XμCT measurement on the as-assembled sample prior to electrochemical operation (pristine), the cell was re-scanned after aging by constant-current/constant-voltage (CCCV) cycling for 20 cycles at a limited cycling window of 20% depth of discharge (DoD; referenced to the cathode capacity, corresponding to

https://doi.org/10.58286/32573

$\approx$ 123 mAh g^{-1} based on MnO_2). Cycling was performed at 0.79 mA (i.e., $\approx$ 1 mA cm^{-2} for the electrode area used; $\approx$ 0.4 C), charging to a cutoff voltage of 1.8 V, and the experiment was terminated with the cell in the fully charged state (SoC = 100%). Electrochemical cycling was carried out using an Arbin MSTAT 5A potentiostat. The sample was made with a custom 3D printed housing and uses brass and graphite current collectors.

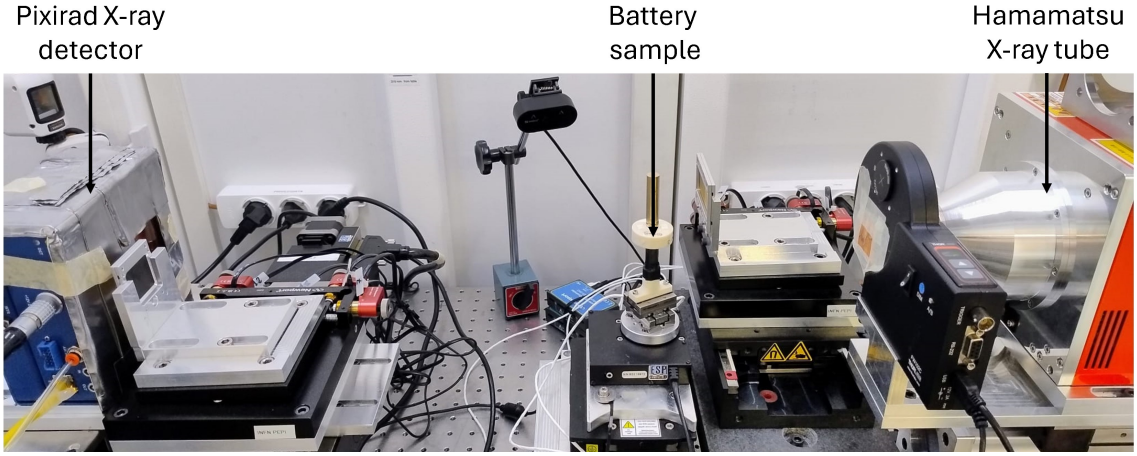

Figure 1: Imaging setup at PEPI Lab. The battery sample has been made with a custom 3D printed housing and uses brass and graphite current collectors.

S-XµCT acquisitions were performed at the PEPI Lab (INFN Trieste) [3] using a photon-counting CdTe spectral detector (Pixirad-PixieIII) with a pixel size of 62 µm along with to a Hamamatsu micro-focus X-ray source (Figure 1). Scans were performed at a magnification of 3×, corresponding to an effective voxel size of 20 µm. For each scan, 720 projection images were acquired over a full 360° rotation, with an exposure time of 9 s per projection. Each projection was acquired twice using two pairs of detector energy thresholds, similarly to what is reported in [4]: 35.0 keV and 50.0 keV for the first acquisition, followed by 70.0 keV and 90.5 keV for the second. The X-ray source was operated at 100 kVp and 200 µA, and the beam was filtered by 1.75 mm of Al and 0.6 mm of Cu, in addition to the 0.15 mm Be window. The total acquisition time for each sample was approximately 6 h.

Prior to reconstruction, the projection data were preprocessed and separated into four energy-bin datasets defined by the detector thresholds: 35.0–50.0 keV, 50.0–70.0 keV, 70.0–90.5 keV, and $>$ 90.5 keV, where the last energy bin is chosen to exceed the bismuth K-edge (90.5 keV). Each energy-bin dataset was reconstructed independently using the Feldkamp algorithm with a cosine filter. In addition, a high-statistics attenuation reconstruction was generated by summing all energy bins above 35 keV. Material decomposition was subsequently performed on the reconstructed datasets, yielding three-dimensional material concentration volumes corresponding to three selected basis materials: carbon (C), manganese (Mn), and bismuth (Bi). It should be noted that although the decomposed material values have the physical dimension of mass density (g/cm^3), the reported absolute values should be considered a first-order approximation, as no system calibration was performed using a test phantom with known material densities. Nevertheless, because experimental conditions and the parameters of the decomposition algorithm were kept constant across acquisitions, relative comparisons between different samples remain reliable. Moreover, analysis of the attenuation reconstructions across different energy intervals reveals an increase in attenuation in the highest energy bin, i.e., above the bismuth K-edge, localized at the bismuth clusters. As illustrated by the example in Figure 2, this behavior constitutes a clear signature of the presence of bismuth.

Table 1: Stability of the spectral technique

	Att. bin 1 (cm^{-1})	**Carbon (g/cm^3)**	**Manganese (g/cm^3)**	**Bismuth (g/cm^3)**
Test 1	0.937	1.950	0.252	0.025
Test 2	0.932	1.848	0.241	0.029
Test 3	0.924	1.745	0.230	0.033
Test 4	0.963	1.901	0.243	0.030
Mean (μ)	0.939	1.861	0.241	0.029
Std (σ)	0.017	0.088	0.009	0.003
σ/μ (%)	1.8%	4.7%	3.8%	10.9%

To evaluate the stability and reproducibility of the entire spectral imaging and material decomposition process, repeated acquisitions were performed on the same battery sample under identical experimental conditions over a period of one week. Four

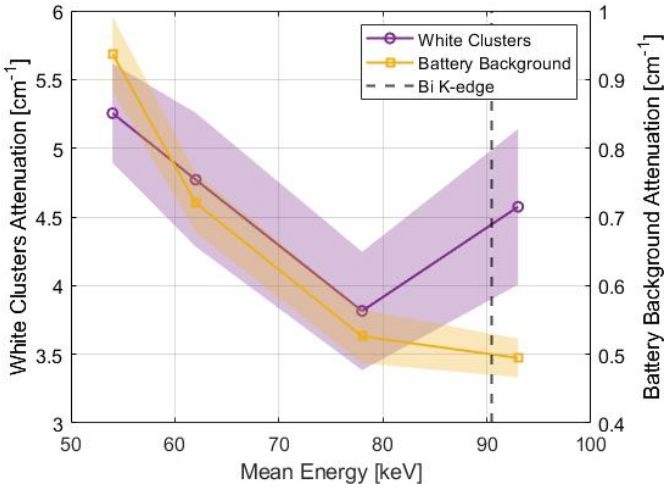

Figure 2: Attenuation of the white clusters (left axis) and the sample background (right axis) as a function of the mean energy of each bin. The attenuation of the clusters increases in the highest energy bin, consistent with K-edge of Bi.

independent scans were acquired and processed using the same reconstruction and decomposition pipeline. For each dataset, a fixed region of interest (ROI) was selected within the active region of the battery, and the mean value and standard deviation were calculated over ten consecutive slices. This procedure was applied to the attenuation reconstruction as well as to each material decomposition channel, which are shown in Figure 3. The resulting relative errors (σ/μ) were below 5% for the attenuation, carbon, and manganese channels, while the bismuth channel exhibited a slightly higher relative error of 10.9% (Table 1). These results indicates the level of stability and reproducibility of the S-XμCT acquisition and decomposition process for this particular sample and time-scale. From the three material images in Figure 3, it can also be observed that signal contamination is present across all three material channels on the left side of the sample, corresponding to the highly attenuating zinc anode. Consequently, the ROIs were restricted to the central region of the sample and to slices that do not include the zinc anode.

Based on preliminary inspection of the reconstructed attenuation volumes and material-specific channels, the subsequent analysis focused on the attenuation reconstruction and the bismuth material channel, as these exhibited the most pronounced clustering behavior. Both quantitative analysis and qualitative inspection were performed to investigate the spatial distribution of clusters as a function of distance from the anode interface.

The pristine and aged datasets were first spatially aligned by visual inspection, using the position of the boundary between the anode and the active cathode region as a reference. After registration, image analysis was performed using Fiji (ImageJ). Starting from the slice immediately adjacent to the anode boundary, clusters were identified using intensity thresholding to isolate regions of elevated signal. The lower threshold was set to 0.16 cm^{-1} for the attenuation datasets and to 0.13 g/cm^3 for the bismuth channel, both values tuned manually to effectively isolate the clusters from the background. Cluster identification was carried out using the *Analyze Particles* function. Features were classified as clusters if they occupied between 4 and 500 voxels, and a minimum circularity of 0.5 was imposed to suppress irregularly shaped features that may be associated with imaging artifacts or intrinsic electrode inhomogeneities. Identical analysis parameters were applied to both the pristine and aged datasets to ensure direct comparability.

3 Results

Figure 4 summarizes the quantitative analysis of the S-XμCT data obtained from the pristine and aged battery samples. The number of identified clusters is shown as a function of distance from the anode interface for both the attenuation reconstruction (top left panel) and the bismuth material channel (top right panel). In both datasets, the aged battery exhibits a pronounced increase in cluster density in the vicinity of the anode boundary. At larger distances from the anode interface (greater than approximately 600 μm), the number of detected clusters in the pristine and aged samples converges to more similar values.

While this trend is observed in both datasets, the contrast between pristine and aged samples is more pronounced in the bismuth channel than in the attenuation reconstruction. In the bismuth channel, the aged sample exhibits a very large relative increase in cluster counts close to the anode interface, reflecting the near absence of detectable bismuth clusters in the pristine sample. Specifically, relative increases between the aged and pristine datasets of approximately 7300% at 300 μm and 500% at 600 μm from the anode interface are observed. By comparison, the attenuation dataset shows increases of approximately 340% at 300 μm and 200% at 600 μm. These results suggests an enhanced sensitivity of the spectral decomposition approach for identifying bismuth clusters relative to conventional attenuation-based imaging. Indeed, a very small number of bismuth clusters (< 3) is consistently observed throughout the pristine sample dataset indicating its robustness. It should be noted that the increase in the bismuth cluster counts of the pristine battery at around 200 μm depth is attributed to localized image artifact rather than bismuth

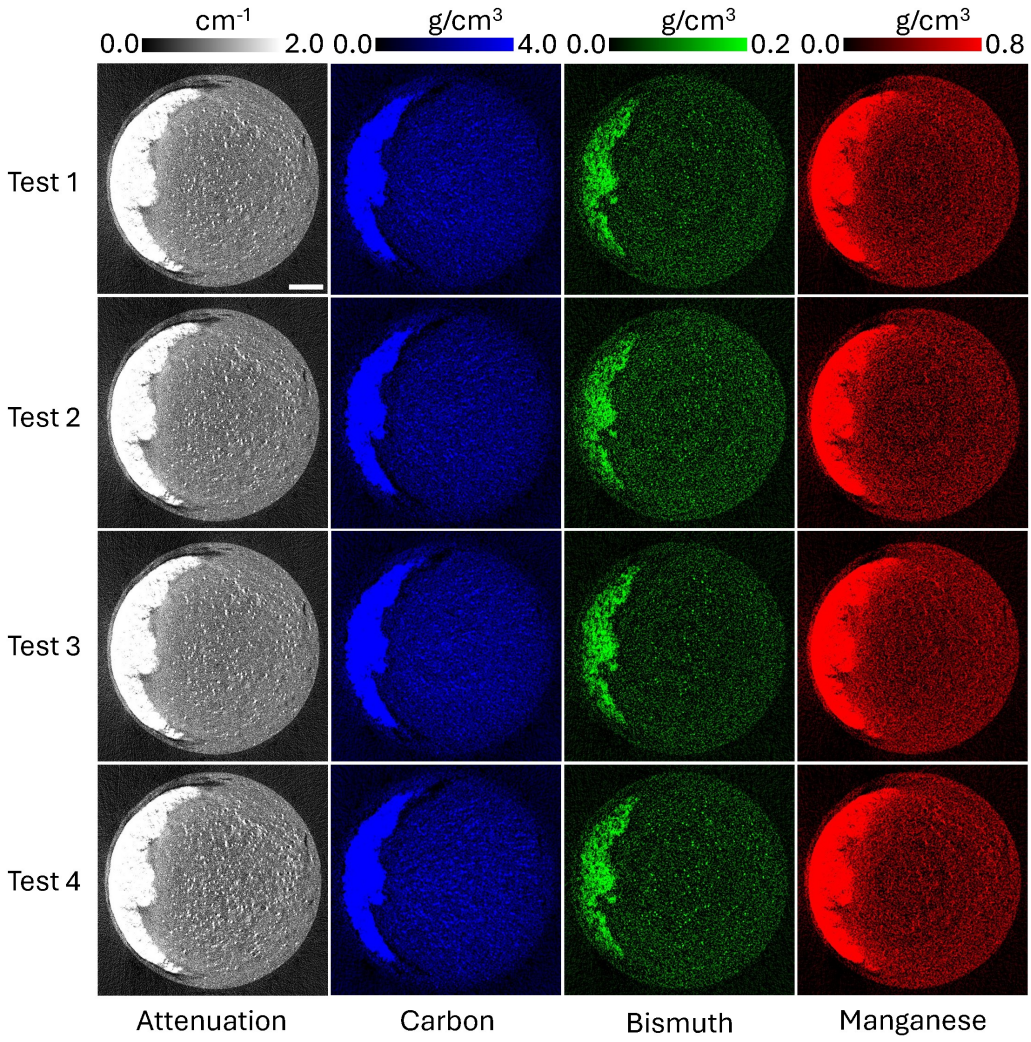

Figure 3: Stability of spectral technique. The attenuation images (first column), carbon channel images (second column), bismuth channel images (third column), and manganese channel images (fourth column) for all the repeated acquisitions (rows) are shown. Scale bar corresponds to 2 mm.

clusters.

The bottom panels of Figure 4 show the mean attenuation signal (bottom left) and the bismuth concentration (bottom right) within clusters across the sample. While differences are observed in the number of clusters between pristine and aged sample scans, no major variations are evident in the mean cluster values, indicating that battery aging primarily affects cluster formation, namely their number, rather than their composition.

These quantitative trends are further illustrated qualitatively in Figure 5, which presents representative attenuation and bismuth-channel slices extracted at depths of 600 µm and 300 µm from the anode interface for both pristine and aged samples. At a depth of 600 µm, the number and spatial distribution of clusters appear similar in the pristine and aged datasets for both imaging modalities. In contrast, at a depth of 300 µm, a marked increase in the number of clusters is observed in the aged sample in both the attenuation and bismuth images. These observations are consistent with the quantitative analysis and indicate that ageing-induced clustering is strongly localized near the anode interface.

To better visualize this effect, a 3D rendering of the reconstructed volumes was generated to provide a global visualization of the battery samples and the corresponding spatial distribution of the ageing-induced clusters (Figure 6). The 3D rendering reveals a visibly higher concentration in bismuth clusters in the region proximal to the anode interface in the aged sample. In contrast, the pristine sample exhibits a more uniform appearance, with few clusters. These volumetric visualizations are consistent with the slice-based quantitative and qualitative analyses and provide complementary insight into the three-dimensional extent and spatial organization of clustering phenomena within the electrode.

The observed ageing-induced formation of Bi-containing clusters is in line with the dissolution/precipitation processes, that can explain the available electrochemical results and ex situ SEM/EDS imaging of cathodes extracted from cycled batteries. In fact, evenly-distributed micron-sized Bi_2O_3 grains, present in the as-fabricated samples, can hardly be discerned under the imaging

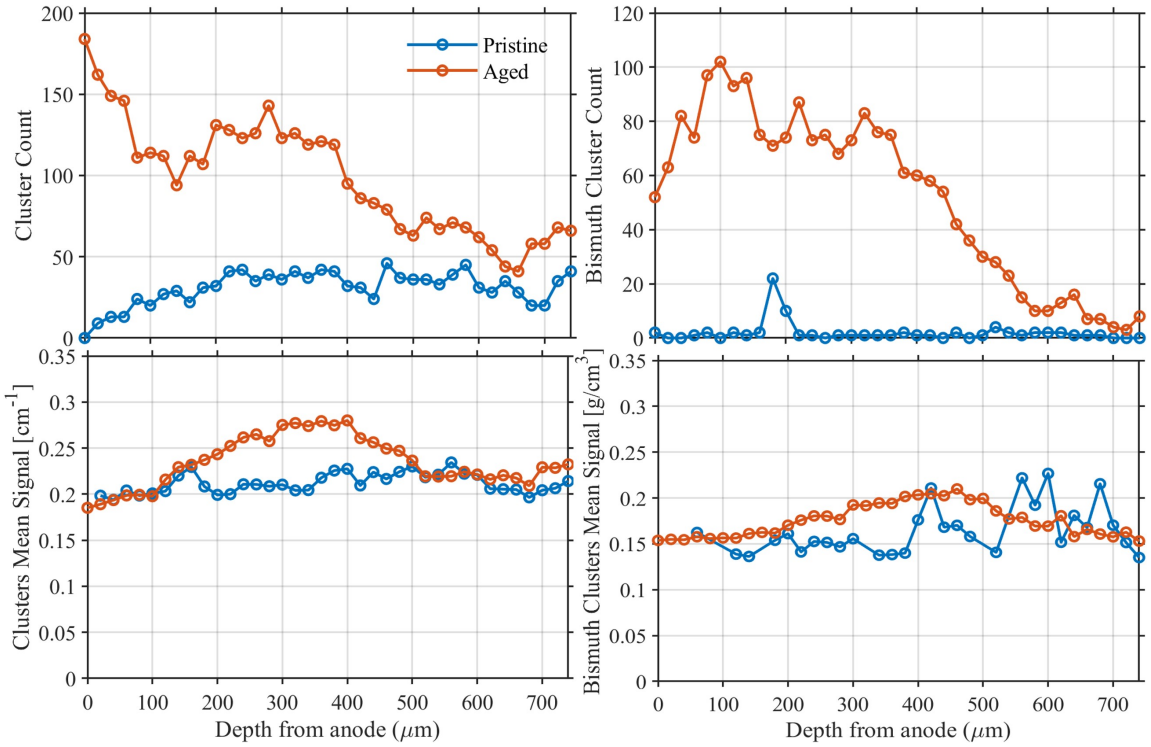

Figure 4: Quantitative comparison between the pristine and aged battery sample. The number of identified clusters (top) and the mean signal in each cluster (bottom) are shown for both the attenuation dataset (left) and bismuth channel dataset (right).

conditions of this work. Nevertheless, reductive Mn dissolution and Bi reduction during discharge, followed by Bi oxidative dissolution and Mn oxidative precipitation in the recharge cycle, is expected to lead to the precipitation of both Mn- and Bi-oxide clusters, that, in principle, can grow to dimension that make them detectable by micro-CT. Importantly, the homogeneous Bi distribution observed in the aged sample, exhibiting extensive clustering, is a piece of evidence in favour of the formation of mixed Mn-Bi oxide phases, currently postulated on the basis of electroanalytical data. The increasing tendency to clustering close to the anode clearly correlates with the higher cathode activity at the electrode/electrolyte interface, resulting from penetration of current density in the 3D composite electrode.

4 Conclusion

In this work, spectral X-ray micro-computed tomography was employed to investigate pristine and aged Mn-Bi-based rechargeable alkaline batteries. The technique enables non-destructive, three-dimensional characterization of both morphological and compositional changes associated with battery ageing. Through material decomposition, improved discrimination of bismuth clusters relative to conventional attenuation-based imaging was achieved, enabling enhanced quantification of ageing-induced features and improved insight into their spatial distribution with respect to the anode interface.

Stability and reproducibility testing confirmed the robustness of the S-XμCT acquisition and material decomposition workflow at the PEPI Lab, confirming that the observed differences between pristine and aged samples arise from the ageing process itself rather than experimental variability. Quantitative analysis revealed a pronounced increase in the number of clusters in the aged battery, with this effect being strongly localized near the anode interface. At the same time, mean cluster signal analysis, suggested that no relevant differences in the cluster content are present. These trends were observed in both the attenuation and bismuth datasets, with the spectral bismuth channel providing improved relative discrimination between the aged and pristine samples. Complementary three-dimensional renderings further illustrated the spatial distribution of ageing-induced bismuth clusters throughout the cathode volume.

Future work will focus on extending the analysis to larger sample sets and on correlating S-XμCT-derived metrics with battery cycling parameters, such as: voltage cutoffs, recharge strategies featuring mixed potential-current control, depth of discharge/charge and discharge/charge rate. Moreover, the capability of following the clustering gradient along the cathode thickness is a valuable tool for the optimization of cathode architecture, in view of approximating the ideal condition whereby each elementary volume would exhibits the same electrochemical activity, enabling full exploitation of the active material.

Acknowledgements

We acknowledge funding by the Italian Ministry of University and Research (MUR) under National Recovery and Resilience Plan (PNRR), funded by the European Union – NextGenerationEU – Project P2022X5ALY – CUP J53D23014070001. EM

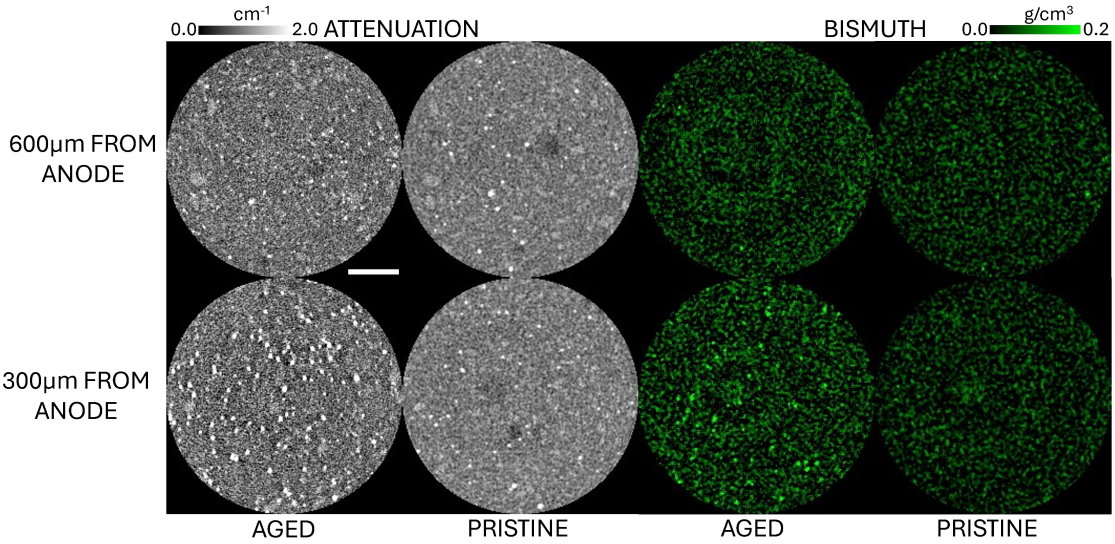

Figure 5: Qualitative comparison between the pristine and aged battery sample for both attenuation (gray) and bismuth images (green), at 600 μm and 300 μm depth from the anode. The regions correspond to the ROIs used for the quantitative analysis shown in Figure 4. Scale bar corresponds to 1 mm.

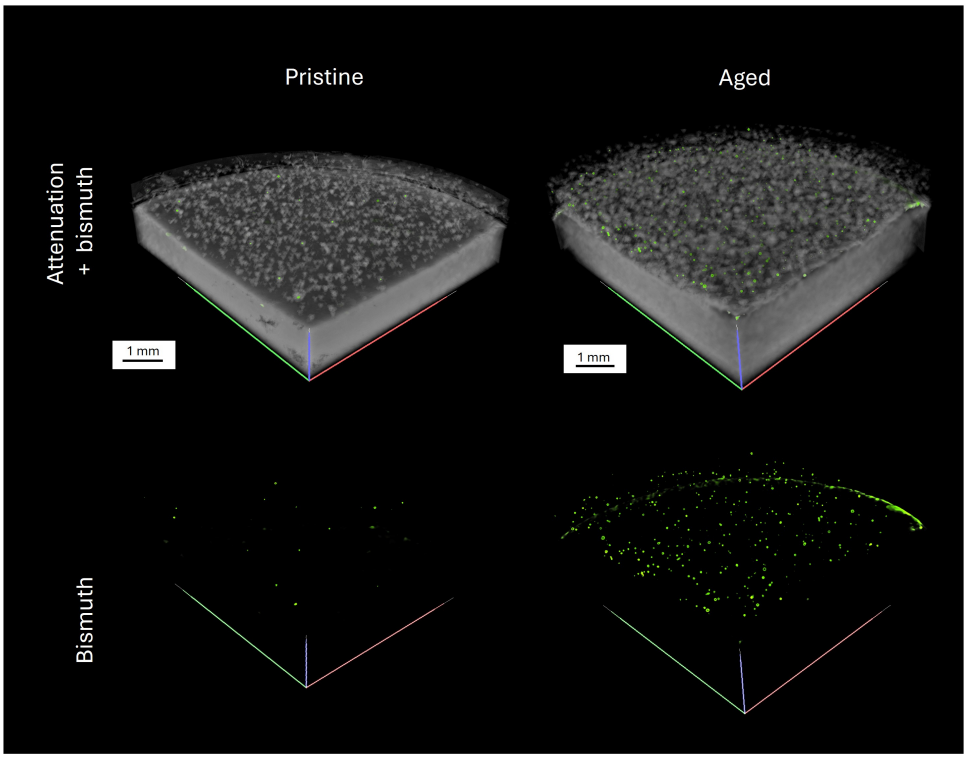

Figure 6: A 3D rendering of the pristine (left) and aged (right) battery sample. The aged sample exhibits increased bismuth clustering near the anode interface.

and RH aknoledge funding by the Bundesministerium für Forschung, Technologie und Raumfahrt (BMFTR), Project number 03XP0570A. We acknowledge Jannis Schindling for his support with preliminary cathode fabrication and electrochemical testing.

References

[1] U. Rojas-Alva, L. Mancini, A. M. Pranjić, E. Marini, B. Bozzini, On thermal safety characteristics of rechargeable alkaline batteries based on zinc and manganese dioxide, Process Safety and Environmental Protection (2025) 107175.

[2] B. Bozzini, I. Sgura, A conceptual, mathematical and quantitative reassessment of the thin-film flooded agglomerate model

for air cathodes, Journal of Electroanalytical Chemistry 950 (2023) 117855.
[3] L. Brombal, F. Arfelli, R. H. Menk, L. Rigon, F. Brun, Pepi lab: a flexible compact multi-modal setup for x-ray phase-contrast and spectral imaging, Scientific Reports 13 (1) (2023) 4206.
[4] V. Di Trapani, L. Brombal, F. Brun, Multi-material spectral photon-counting micro-ct with minimum residual decomposition and self-supervised deep denoising, Optics Express 30 (24) (2022) 42995–43011.